Robustness of Periodic Orbits of Impulsive Systems à la Poincaré

Sushant Veer and Ioannis Poulakakis

***Abstract*— In this paper, we analyze the robustness of distinct periodic solutions of systems with impulse effects (SIEs) under uncertainty through the method of Poincaré. We work with a class of disturbances that affect both the continuous and discrete update dynamics of the SIE, as well as the geometry of the surface governing state transitions. In particular, we show that in the absence of any disturbances, the fixed point of the corresponding Poincaré map is locally asymptotically stable, if, and only if, in the presence of disturbances the periodic orbit of the SIE is locally input-to-state stable. This result generalizes the method of Poincaré for periodic orbits to explicitly incorporate the effect of disturbances. Although our motivation for this work stems from the need to rigorously and conveniently analyze robust controllers for dynamically moving legged robots, the results presented here are relevant to a much broader class of systems that can be modeled as forced SIEs.**

I. Introduction

The method of Poincaré [1] has been one of the principal approaches for investigating the stability properties of isolated periodic orbits, i.e., limit cycles, exhibited by dynamical systems. The method establishes that the asymptotic stability of a periodic orbit is equivalent to the asymptotic stability of the corresponding fixed point of a discrete dynamical system that arises through the associated Poincaré map. In the present paper, we extend the classical Poincaré analysis to analyze the robustness under uncertainty of periodic orbits exhibited by systems with impulse effects (SIEs) [2], using the notion of input-to-state stability (ISS) [3].

SIEs represent a class of hybrid dynamical systems that appear in a wide range of applications, such as impact mechanics [4], population dynamics [5], and legged robotics [6]. Our particular interest in SIEs arises from the latter, where walking and running gaits are abstracted as limit cycle solutions of SIEs. A variety of methods—hybrid zero dynamics [6], geometric reduction [7], and virtual constraints [8] to name a few—have been proposed to generate asymptotically stable limit-cycle solutions to SIEs representing models of periodic locomotion behaviors of legged robots.

Clearly though, in any practical scenario, these robots will have to operate under uncertainty arising through unknown model parameters [9]–[11], ground height variations [12]–[14], as well as exogenous forces [15]–[18]. Frequently, robust locomotion controllers are designed on the basis of the discrete system that arises from a Poincaré map. However, precisely because of the presence of uncertainty, the connection between conclusions obtained by analyzing the fixed point of this discrete system and the periodic solution of the SIE it represents is only partially understood. Addressing this issue is at the core of the present paper.

To study robustness of limit cycles, we adopt the notion of ISS [3], [19]. Analyzing ISS for limit-cycles of SIEs is challenging due to the hybrid nature of the system, and the fact that the 0-input compact attractor is a set rather than an equilibrium point. To address these issues, [20] directly analyzes the solutions of the *hybrid* system using the *point-to-set distance*, which in general settings is a difficult task. By way of contrast, in this paper, and along the lines of Poincaré's method, we exploit the periodicity of the 0-input limit cycle to obtain a discrete dynamical system that encodes its ISS properties, thereby, circumventing the need to study the hybrid solutions of the system under external inputs.

The main contribution of this paper is to prove that, under sufficiently small disturbances, local ISS (LISS) of a hybrid limit cycle of a forced (perturbed) SIE is equivalent to the local ISS of the corresponding 0-input fixed point of the associated *forced Poincaré functional*, which, in turn, is equivalent to the local asymptotic stability (LAS) of this fixed point in the *unforced* Poincaré map. This work extends our recent results in [21] to include disturbances that affect not only the continuous and discrete parts of the SIE, but also the geometry of the surface governing transitions. From a practical perspective, this constitutes an important class of disturbances; a very common example where such disturbances arise is in the study of periodic walking or running on uneven terrain. Finally, it is worth pointing out that the results of this paper are applicable to periodic orbits of continuous-time systems as well by taking the discrete dynamics of the SIE as the identity map.

Notation: The sets of reals and integers are denoted by $\mathbb{R}$ and $\mathbb{Z}$, respectively; the symbols $\mathbb{R}_+$ and $\mathbb{Z}_+$ are used to denote the sets of non-negative reals and integers. For $x \in \mathbb{R}^n$, the Euclidean norm is denoted by $\|x\|$. Let $\mathcal{A} \subseteq \mathbb{R}^n$, then the point-to-set distance of x from $\mathcal{A}$ is defined as $\mathrm{dist}(x, \mathcal{A}) := \inf_{y\in\mathcal{A}} \|x - y\|$. The norm of a continuous function $u : \mathbb{R}_+ \to \mathbb{R}^p$ is defined as $\|u\|_\infty := \sup_{t\in\mathbb{R}_+} \|u(t)\|$, whereas the norm of a sequence $\bar{v} : \mathbb{Z}_+ \to \mathbb{R}^q$ is defined as $\|\bar{v}\|_\infty := \sup_{k\in\mathbb{Z}_+} \|v_k\|$. Despite our use of $\|\cdot\|_\infty$ for the norm of the continuous function as well as the sequence, no confusion arises as it will always be clear from context. A function $\alpha : \mathbb{R}_+ \to \mathbb{R}_+$ belongs to class $\mathcal{K}$ if it is continuous, strictly increasing, and $\alpha(0) = 0$. A function $\beta : \mathbb{R}_+ \times \mathbb{R}_+ \to \mathbb{R}_+$ belongs to class $\mathcal{KL}$ if it is continuous, $\beta(\cdot, t)$ belongs to $\mathcal{K}$ for any fixed $t \geq 0$, $\beta(s, \cdot)$ is strictly

S. Veer is with the Department of Mechanical and Aerospace Engineering, Princeton University, Princeton, NJ 08540, USA, e-mail: sveer@princeton.edu. I. Poulakakis is with the Department of Mechanical Engineering, University of Delaware, Newark, DE 19716, USA; e-mail: poulakas@udel.edu.

This work is supported in part by NSF CAREER Award IIS-1350721 and by NRI-1327614.

decreasing, and $\lim_{t\to\infty}\beta(s,t)=0$, for any fixed $s\geq 0$.

II. Forced Systems with Impulse Effects

The objective of this paper is to analyze the robustness of distinct periodic solutions of forced (perturbed) SIEs. This section introduces and motivates this class of systems.

A. Model Formulation and Motivation

We are interested in SIEs of the form

$$\Sigma:\begin{cases}\dot{x}(t)=f(x(t),u(t)), & \text{if } x(t)\notin\mathcal{S}(w)\\ x(t)^+=\Delta(x(t)^-,v), & \text{if } x(t)^-\in\mathcal{S}(w)\end{cases}, \quad (1)$$

where

$$\mathcal{S}(w):=\{x\in\mathbb{R}^n \mid H(x,w)=0\}\ . \quad (2)$$

In (1) and (2), $x\in\mathbb{R}^n$ denotes the state of the system, and $x(t)^-=\lim_{\tau\nearrow t}x(\tau)$ and $x(t)^+=\lim_{\tau\searrow t}x(\tau)$ are the left- and right-limits of $x(\cdot)$ at t. The continuous-time input signal $u:\mathbb{R}_+\to\mathbb{R}^p$ represents a disturbance that influences the continuous part of (1). In addition, $v\in\mathbb{R}^q$ and $w\in\mathbb{R}^r$ are discrete input values that capture the uncertainty associated with the update rule of (1). We assume that the unforced (0-input) system possesses a limit-cycle solution $\mathcal{O}$ and our goal is to investigate the behavior of $\mathcal{O}$ under the influence of the exogenous continuous and discrete input signals.

Systems like (1) appear naturally in a variety of applications. To provide a concrete example, consider limit-cycle locomotion behaviors in legged robots [6]; see Section VI below for a detailed discussion. Such systems frequently operate under externally applied forces $u(t)$ that are unknown or partially known. Furthermore, there is uncertainty v associated with their state updates as they undergo impact events. Finally, often such robots must walk or run on uneven terrain, resulting in uncertainty regarding ground contacts; in (1) this type of uncertainty is captured by the parameter w affecting the switching conditions. In more general settings, forced SIEs (1) are relevant to studying the robustness of sequentially composed [22] periodic movement primitives [23]–[25] for accomplishing high-level motion planning objectives. In such cases, switching from one movement primitive to another will inevitably involve uncertainty, calling for robustness guarantees [25]. The current paper provides tools for assessing robustness of the individual primitives.

B. Modeling Assumptions

We require the following assumptions.

A.1) $f:\mathbb{R}^n\times\mathbb{R}^p\to\mathbb{R}^n$ is twice continuously differentiable

A.2) u belongs to the space of continuous bounded functions $\mathcal{U}:=\{u:\mathbb{R}_+\to\mathbb{R}^p \mid u \text{ is continuous, } \|u\|_\infty<\infty\}$

Assumption A.1, the continuity of u as a function of t by assumption A.2, and [26, Theorem 3.1] guarantee the local existence and uniqueness of the flow $\varphi(t,x(0),u)$ of the continuous-time part of (1), which starts from the initial state $x(0)$ and evolves under the influence of a fixed u.

The continuous-time evolution of (1) terminates when the flow φ intersects the surface $\mathcal{S}(w)$ defined by (2). We assume

A.3) $H:\mathbb{R}^n\times\mathbb{R}^r\to\mathbb{R}$ is twice continuously differentiable. Furthermore, there exists $\delta_w>0$ such that for any $\hat{w}\in B_{\delta_w}(0)$ and for any $\hat{x}\in\mathcal{S}(\hat{w})$ we have $\frac{\partial H}{\partial x}|_{(\hat{x},\hat{w})}\neq 0$.

Assumption A.3 ensures that for each $w\in B_{\delta_w}(0)$, the switching surface $\mathcal{S}(w)$ defined by (2) is a co-dimension 1 embedded sub-manifold of $\mathbb{R}^n$ [1, p. 431]. Intuitively, we can view w as a disturbance which "deforms" and "moves" the switching surface in $\mathbb{R}^n$ while retaining its smooth structure.

The hybrid flow of (1) can be constructed by the flow φ of the continuous-time part of (1) which, on approaching $\mathcal{S}(w)$, is interrupted by the update map Δ, for which we assume

A.4) $\Delta:\mathbb{R}^n\times\mathbb{R}^q\to\mathbb{R}^n$ is twice continuously differentiable

Now, let $x(t):=\psi(t,x(0),u,\bar{v},\bar{w})$ be the hybrid flow of (1) from the initial state $x(0)$, evolving under the continuous-time input $u\in\mathcal{U}$, and the sequence of input values $\bar{v}:\mathbb{Z}_+\to\mathbb{R}^q$ and $\bar{w}:\mathbb{Z}\to\mathbb{R}^r$ that perturb the update law Δ and "deform" the surface $\mathcal{S}(w)$. We will assume that

A.5) $\bar{v}\in\mathcal{V}:=\{\bar{v}:\mathbb{Z}_+\to\mathbb{R}^q \mid \|\bar{v}\|_\infty<\infty\}$ and $\bar{w}\in\mathcal{W}:=\{\bar{w}:\mathbb{Z}\to\mathbb{R}^r \mid \|\bar{w}\|_\infty<\infty\}$

Let $x^*\in\mathcal{S}(0)$ and $T^*\in(0,\infty)$ be such that

A.6) $\mathrm{dist}(\Delta(x^*,0),\mathcal{S}(0))>0$ and $\varphi(t,\Delta(x^*,0),0)$ exists for all $t\in[0,T^*]$.

Then we can define the set

$$\mathcal{O}:=\{\varphi(t,\Delta(x^*,0),0) \mid t\in[0,T^*)\}\ , \quad (3)$$

for which we assume that

A.7) $\overline{\mathcal{O}}\cap\mathcal{S}(0)=\{x^*\}$ and $\mathcal{O}$ is transversal to $\mathcal{S}(0)$ at x^*, i.e., $L_fH(x^*,0,0)<0$.

With these assumptions, it follows that $\mathcal{O}$ is a periodic orbit of (1) in the absence of any external inputs and x^* corresponds to its geometric intersection with $\mathcal{S}$.

III. Augmented Forced Poincaré Map

We are interested in the behavior of the unforced periodic solution $\mathcal{O}$ defined by (3) in the presence of the (possibly non-vanishing) perturbations u, v and w. Our analysis will be based on the notion of a *forced* Poincaré map, which returns the next intersection of the *forced* solution of a system with a suitably defined Poincaré section. Note that when $w=0$, the (unperturbed) surface $\mathcal{S}(0)$ serves as a natural (albeit not unique) choice for a Poincaré section [21, p. 3]. However, in the presence of a non-zero perturbation w, the switching surface varies at each discrete event. Note here that some other surface that is transversal to the orbit could be selected as a section where the solution is sampled. However, in a practical setting, there will always be uncertainty associated with any choice of this section due to sensor noise or other sources. In what follows, and without loss of generality, we will select the switching surface of (1) to sample the solution. Hence, before defining the forced Poincaré map, we reformulate the SIE (1) in an augmented form which facilitates subsequent analysis.

Consider the evolution of the system between two successive crossings of the switching surface; see Fig. 1. We adopt the following conventions. Let t_k be the time instant of crossing the surface $\mathcal{S}_k=\mathcal{S}(w_{k-1})$ determined by the input value

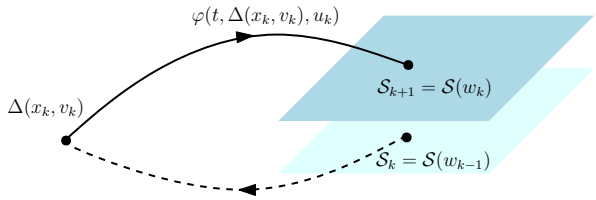

Fig. 1. Solution of (1) evolves from $\mathcal{S}_k$ to $\mathcal{S}_{k+1}$. Dashed line corresponds to the discrete dynamics, while the solid line represents the evolution during the continuous phase.

$w_{k-1} \in \bar{w}$ and let $x_k = \lim_{t \nearrow t_k} x(t)$ be the corresponding state just prior to intersecting $\mathcal{S}_k$. The update rule $\Delta(x_k, v_k)$ provides initial conditions for the subsequent continuous evolution $x(t) = \varphi(t, \Delta(x_k, v_k), u(t))$ for $t \geq t_k$, and the system continues until it crosses the surface $\mathcal{S}_{k+1} = \mathcal{S}(w_k)$. To capture the discrete evolution of the switching surfaces, we define a new state variable $s \in \mathbb{R}^r$ with dynamics $\dot{s} = 0$ between successive crossings. In addition, at each crossing, the state s is updated to the value w that determines the next crossing. Hence, $s(t)$ is a piecewise-constant, right-continuous signal and $\lim_{t \nearrow t_k} s(t) = s_k = w_{k-1}$ with $\mathcal{S}_k = \mathcal{S}(w_{k-1})$ being the most recently intersected surface and $\lim_{t \searrow t_k} s(t) = \Delta_s(w_k) = w_k$, with $\mathcal{S}_{k+1} = \mathcal{S}(w_k)$ being the surface that determines the next switching.

This way, we can define an augmented SIE with state $x_{\mathrm{a}} := (x, s) \in \mathbb{R}^n \times \mathbb{R}^r$ and dynamics

$$\Sigma_{\mathrm{a}} : \begin{cases} \dot{x}_{\mathrm{a}}(t) = f_{\mathrm{a}}(x_{\mathrm{a}}(t), u(t)), & \text{if } x_{\mathrm{a}}(t) \notin \mathcal{S}_{\mathrm{a}} \\ x_{\mathrm{a}}^+ = \Delta_{\mathrm{a}}(x_{\mathrm{a}}^-, v, w), & \text{if } x_{\mathrm{a}}^- \in \mathcal{S}_{\mathrm{a}} \end{cases} , \quad (4)$$

where

$$f_{\mathrm{a}}(x_{\mathrm{a}}, u) := \begin{bmatrix} f(x, u) \\ 0 \end{bmatrix}, \quad \Delta_{\mathrm{a}}(x_{\mathrm{a}}, v, w) := \begin{bmatrix} \Delta(x, v) \\ w \end{bmatrix} \quad (5)$$

and the augmented switching surface is defined as

$$\mathcal{S}_{\mathrm{a}} := \{x_{\mathrm{a}} \in \mathbb{R}^n \times \mathbb{R}^r \mid H(x_{\mathrm{a}}) = 0\} \ . \quad (6)$$

The augmented SIE (4) is in the form of the perturbed SIEs studied in [21] enabling the use of tools provided there.

With this definition of the augmented system, the flow $\varphi_{\mathrm{a}}(t, x_{\mathrm{a}}(0), u)$ of the continuous-time part of (4) takes the form $\varphi_{\mathrm{a}}(t, x_{\mathrm{a}}(0), u) = (\varphi(t, x(0), u), s(0))$. Further, the hybrid flow $x_{\mathrm{a}}(t) := \psi_{\mathrm{a}}(t, x_{\mathrm{a}}(0), u, \bar{v}, \bar{w})$ of (4) satisfies $\psi(t, x(0), u, \bar{v}, \bar{w}) = \Pi_x \psi_{\mathrm{a}}(t, x_{\mathrm{a}}(0), u, \bar{v}, \bar{w})$ where Π_x is the projection of ψ_{a} to its first n components. Hence, the solution of the augmented system retains the solution of (1) while the parameter w that (smoothly) "deforms" the surface $\mathcal{S}(w)$ of (1) enters as a disturbance in the discrete dynamics of the augmented system. With these constructions,

$$\mathcal{O}_{\mathrm{a}} := \mathcal{O} \times \{0\} \subset \mathbb{R}^n \times \mathbb{R}^r \ , \quad (7)$$

is a periodic orbit of (4) that satisfies assumptions A.6-A.7 with respect to the dynamics of the augmented SIE (4).

To analyze the behavior of $\mathcal{O}_{\mathrm{a}}$ under the influence of the external inputs $u, \bar{v}, \bar{w}$, we now define the forced Poincaré map. We begin by introducing the time-to-impact map $T_{\mathrm{I}} : \mathcal{S}_{\mathrm{a}} \times \mathcal{U} \times \mathbb{R}^q \times \mathbb{R}^r \to \mathbb{R}_+$,

$$T_{\mathrm{I}}(x_{\mathrm{a}}, u, v, w) := \begin{cases} \inf\{t \geq 0 | \varphi_{\mathrm{a}}(t, \Delta_{\mathrm{a}}(x_{\mathrm{a}}, v, w), u) \in \mathcal{S}_{\mathrm{a}}\}, \\ \qquad \text{if } \exists t : \varphi_{\mathrm{a}}(t, \Delta_{\mathrm{a}}(x_{\mathrm{a}}, v, w), u) \in \mathcal{S}_{\mathrm{a}} \\ \infty, \quad \text{otherwise} \end{cases} \quad (8)$$

that provides the time required by the flow of (4) starting at $x_{\mathrm{a}} \in \mathcal{S}_{\mathrm{a}}$ and evolving under u, v, and w, to return to $\mathcal{S}_{\mathrm{a}}$. The forced Poincaré map $P_{\mathrm{a}} : \mathcal{S}_{\mathrm{a}} \times \mathcal{U} \times \mathbb{R}^q \times \mathbb{R}^r \to \mathcal{S}_{\mathrm{a}}$ is then defined by

$$P_{\mathrm{a}}(x_{\mathrm{a}}, u, v, w) := \varphi_{\mathrm{a}}(T_{\mathrm{I}}(x_{\mathrm{a}}, u, v, w), \Delta_{\mathrm{a}}(x, v, w), u), \quad (9)$$

Observe that T_{I} in (8) depends on the *function* of time u, which by assumption A.2 belongs in the space of continuous bounded functions. Hence, T_{I}, and consequently P_{a}, are nonlinear *functionals* defined on an infinite-dimensional Banach space. Although, due to space limitations, we point to [21] for a detailed treatment of such objects, we mention here that by an argument similar to that in the proof of [21, Lemma 1] the existence of a $\delta > 0$ can be established so that $T_{\mathrm{I}}(x_{\mathrm{a}}, u, v, w)$ is continuously (Fréchet) differentiable in its arguments for any $x_{\mathrm{a}} \in B_\delta(x_{\mathrm{a}}^*)$ where $x_{\mathrm{a}} := (x^*, 0)$, $u \in \mathcal{U}$ such that $\|u\|_\infty < \delta$, $v \in B_\delta(0)$, and $w \in B_\delta(0)$. From the continuous differentiability of φ_{a} [21, Lemma 1] and T_I it follows that P_{a} is continuously differentiable in its arguments for similar neighborhoods as T_{I}.

The augmented forced Poincaré map gives rise to a discrete dynamical system, which evolves on $\mathcal{S}_{\mathrm{a}}$ and has the following structure

$$\begin{bmatrix} x_{k+1} \\ s_{k+1} \end{bmatrix} = \begin{bmatrix} P(x_k, u_k, v_k, w_k) \\ w_k \end{bmatrix} \ , \quad (10)$$

where according to our convention (x_k, s_k) denotes the state of the augmented system just prior to intersecting $\mathcal{S}_{\mathrm{a}}$ and $u_k := u|_{[t_k, t_{k+1})}$ is the restriction of u on the interval $[t_k, t_{k+1})$. Finally, the unforced (zero-input) fixed point $x_{\mathrm{a}}^* := (x^*, 0)$ represents the limit cycle $\mathcal{O}_{\mathrm{a}}$.

Note that by the structure of the augmented system, the map P in (10) does not depend on the s-component of the augmented state and the two parts are decoupled. Hence, x^* is a zero-input fixed point of the system

$$x_{k+1} = P(x_k, u_k, v_k, w_k) \ , \quad (11)$$

that is $x^* = P(x^*, 0, 0, 0)$. Finally, we note that the unforced Poincaré map $P_0 : \mathcal{S}(0) \to \mathcal{S}(0)$, i.e., $u = 0$, $\bar{v} \equiv 0$, and $\bar{w} \equiv 0$, can be recovered by $P_0(x) := P(x, 0, 0, 0)|_{\mathcal{S}(0)}$, and gives rise to a discrete dynamical system

$$x_{k+1} = P_0(x_k) \ , \quad (12)$$

with x^* as its fixed point.

IV. Main Results

To present the main result of the paper, we will need the following stability definitions.

Definition 1: The 0-input periodic orbit $\mathcal{O}$ of (1) is orbitally LISS if there exist $\delta > 0$, $\alpha_1, \alpha_2, \alpha_3 \in \mathcal{K}$, and $\beta \in \mathcal{KL}$, such that $x(t) := \psi(t, x(0), u, \bar{v}, \bar{w})$ satisfies for all $t \geq 0$,

$$\begin{aligned}\operatorname{dist}(x(t), \mathcal{O}) \leq \beta(\operatorname{dist}(x(0), \mathcal{O}), t) + \alpha_1(\|u\|_\infty) \\ + \alpha_2(\|\bar{v}\|_\infty) + \alpha_3(\|\bar{w}\|_\infty) \ , \end{aligned} \tag{13}$$

for any[1] $x(0) \in \mathcal{S}_0^+$ with $\operatorname{dist}(x(0), \mathcal{O}) < \delta$, $u \in \mathcal{U}$ with $\|u\|_\infty < \delta$, $\bar{v} \in \mathcal{V}$ with $\|\bar{v}\|_\infty < \delta$, and $\bar{w} \in \mathcal{W}$ with $\|\bar{w}\|_\infty < \delta$.

Definition 2: The fixed point x^* of (12) is LAS if there exist a $\delta > 0$ and $\beta \in \mathcal{KL}$, such that for all $k \in \mathbb{Z}_+$,

$$\|x_k - x^*\| \leq \beta(\|x_0 - x^*\|, k) \ , \tag{14}$$

holds for any $x_0 \in B_\delta(x^*)$.

Definition 3: The 0-input fixed point x^* of (11) is LISS if there exist $\delta > 0$, $\alpha_1, \alpha_2, \alpha_3 \in \mathcal{K}$, and $\beta \in \mathcal{KL}$, such that for all $k \in \mathbb{Z}_+$,

$$\begin{aligned}\|x_k - x^*\| \leq \beta(\|x_0 - x^*\|, k) + \alpha_1(\|u\|_\infty) + \alpha_2(\|\bar{v}\|_\infty) \\ + \alpha_3(\|w\|_\infty) \ , \end{aligned} \tag{15}$$

is satisfied for any $x_0 \in \mathcal{S}_0 \cap B_\delta(x^*)$, $u \in \mathcal{U}$ with $\|u\|_\infty < \delta$, $\bar{v} \in \mathcal{V}$ with $\|\bar{v}\|_\infty < \delta$, and $\bar{w} \in \mathcal{W}$ with $\|\bar{w}\|_\infty < \delta$.

With the above definitions, we are now ready to state the main result of this paper.

Theorem 1: Consider the SIE (1) and the discrete dynamical systems (10) and (12). Let assumptions A.1-A.7 in Section II be satisfied. Then, the following are equivalent:

(i) fixed point x^* of (12) is LAS;
(ii) 0-input fixed point x^* of (11) is LISS;
(iii) 0-input orbit $\mathcal{O}$ of (1) is LISS.

The practical significance of Theorem 1 lies in the fact that it substantially simplifies the assessment of LISS of periodic orbits of SIEs in the presence of uncertainty. If the uncertainty can be represented in the form of disturbances affecting both the continuous and discrete parts as well as the switching surface of the SIE (1), then proving orbital LISS of a periodic solution of interest reduces to evaluating the asymptotic stability properties of the corresponding fixed point of the discrete dynamical system (12). In fact, the design of control laws for enhancing the robustness of a fixed point of (12) can be directly related to the orbital setting of (1) in the sense that the corresponding periodic orbit will be LISS for sufficiently small (orbital) disturbances.

V. Proof of Theorem 1

The proof of Theorem 1 relies on the results in [21] and is organized in a sequence of lemmas, the purpose of which is to show that the following statements are equivalent:

(a) 0-input fixed point x_{a}^* of (10) is LAS,
(b) 0-input fixed point x_{a}^* of (10) is LISS,
(c) 0-input orbit $\mathcal{O}_{\mathrm{a}}$ of (4) is LISS,
(d) 0-input orbit $\mathcal{O}$ of (1) is LISS,
(e) 0-input fixed point x^* of (11) is LISS,
(f) fixed point x^* of (12) is LAS.

The first lemma establishes bounds[2] relating "distances" from periodic solutions of (4) and (1).

Lemma 1: Let $\mathcal{O}$ and $\mathcal{O}_{\mathrm{a}}$ be defined as in (3) and (7), respectively. Then, for any $x_{\mathrm{a}} := (x, s) \in \mathbb{R}^n \times \mathbb{R}^r$ and any $y_{\mathrm{a}} := (y, \hat{s}) \in \mathbb{R}^n \times \mathbb{R}^r$,

(i) $\|x - y\| \leq \|x_{\mathrm{a}} - y_{\mathrm{a}}\| \leq \|x - y\| + \|s - \hat{s}\|$,
(ii) $\operatorname{dist}(x, \mathcal{O}) \leq \operatorname{dist}(x_{\mathrm{a}}, \mathcal{O}_{\mathrm{a}}) \leq \operatorname{dist}(x, \mathcal{O}) + \|s\|$.

Proof: The first inequality of *(i)* follows by noting that $x - y$ is the projection of $x_{\mathrm{a}} - y_{\mathrm{a}}$ on its first n coordinates, while the second inequality follows by triangle inequality.

To prove *(ii)*, note that by the definition of $\mathcal{O}_{\mathrm{a}}$ in (7), $y_{\mathrm{a}} \in \mathcal{O}_{\mathrm{a}}$ takes the form of $(y, 0)$ where $y \in \mathcal{O}$. Hence,

$$\operatorname{dist}(x_{\mathrm{a}}, \mathcal{O}_{\mathrm{a}}) := \inf_{y_{\mathrm{a}} \in \mathcal{O}_{\mathrm{a}}} \|x_{\mathrm{a}} - y_{\mathrm{a}}\| = \inf_{y \in \mathcal{O}} \|(x, s) - (y, 0)\|. \tag{16}$$

As $\|x - y\| \leq \|(x, s) - (y, 0)\|$, we get,

$$\begin{aligned}\operatorname{dist}(x, \mathcal{O}) = \inf_{y \in \mathcal{O}} \|x - y\| &\leq \inf_{y \in \mathcal{O}} \|(x, s) - (y, 0)\| \\ &= \operatorname{dist}(x_{\mathrm{a}}, \mathcal{O}_{\mathrm{a}}) \ , \end{aligned}$$

where the last equality follows from (16), completing the proof of the first inequality of *(ii)*. Now, using the second inequality of Lemma 1*(i)* in (16), we get

$$\operatorname{dist}(x_{\mathrm{a}}, \mathcal{O}_{\mathrm{a}}) \leq \inf_{y \in \mathcal{O}} \|x - y\| + \|s\| = \operatorname{dist}(x, \mathcal{O}) + \|s\| \ ,$$

completing the proof of the second inequality of *(ii)*. ■

Lemma 2: (a) $\iff$ (b) $\iff$ (c)

Proof: The proof of this lemma relies on the results in [21] given the structure of the augmented SIE (4). From assumptions A.1-A.7 in Section II, it can be verified that (4) satisfies [21, Assumptions A.1-A.3] and that the augmented orbit $\mathcal{O}_{\mathrm{a}}$ satisfies [21, Assumptions A.4-A.7]. Hence, [21, Theorem 2] gives (a) $\iff$ (b) followed by [21, Theorem 1] which shows that (b) $\iff$ (c), completing the proof. ■

Lemma 3: (c) $\iff$ (d)

Proof: Let $x(t)$ and $x_{\mathrm{a}}(t)$ be solutions of (1) and (4), respectively, as discussed below (4).

($\implies$) Assume that (c) holds. Using the first inequality of Lemma 1*(ii)*, for all $t \geq 0$,

$$\begin{aligned}\operatorname{dist}(x(t), \mathcal{O}) &\leq \operatorname{dist}(x_{\mathrm{a}}(t), \mathcal{O}_{\mathrm{a}}) \\ &\leq \beta(\operatorname{dist}(x_{\mathrm{a}}(0), \mathcal{O}_{\mathrm{a}}), t) + \alpha_1(\|\bar{u}\|_\infty) \\ &\quad + \alpha_2(\|\bar{v}\|_\infty) + \alpha_3(\|\bar{w}\|_\infty) \\ &\leq \beta(\operatorname{dist}(x(0), \mathcal{O}) + \|s(0)\|, t) + \alpha_1(\|\bar{u}\|_\infty) \\ &\quad + \alpha_2(\|\bar{v}\|_\infty) + \alpha_3(\|\bar{w}\|_\infty) \\ &\leq \beta(2\operatorname{dist}(x(0), \mathcal{O}), t) + \alpha_1(\|\bar{u}\|_\infty) \\ &\quad + \alpha_2(\|\bar{v}\|_\infty) + \alpha_3(\|\bar{w}\|_\infty) + \beta(2\|\bar{w}\|_\infty, 0) \ , \end{aligned}$$

where the second inequality follows from (c), the third inequality follows from the second inequality of Lemma 1*(ii)*, and the last inequality follows from [27, Lemma 14(2)] with

[1] Without loss of generality, let $\mathcal{S}_{k+1}^+ := \{x \in \mathbb{R}^n \mid H(x, w_k) > 0\}$ be the side of the switching surface where the solution of the SIE evolves after the k-th intersection.

[2] Observe that the bounds of Lemma 1 hold globally; the local nature of the results in subsequent lemmas that use Lemma 1 is inherited by the locality of the corresponding definitions; e.g., Definition 1, 2, or 3.

$\epsilon = 1$ and $\|s(t)\| \leq \|\bar{w}\|_\infty$ for all $t \geq 0$. Finally, noting that $\alpha_3(\|\bar{w}\|_\infty) + \beta(2\|\bar{w}\|_\infty, 0) \in \mathcal{K}$ ensures that (d) holds.
($\Longleftarrow$) Now, assume that (d) holds. Using the second inequality of Lemma 1*(ii)*, for all $t \geq 0$,

$$\begin{aligned}\operatorname{dist}(x_{\mathrm{a}}(t), \mathcal{O}_{\mathrm{a}}) &\leq \operatorname{dist}(x(t), \mathcal{O}) + \|s(t)\| \\ &\leq \beta(\operatorname{dist}(x(0), \mathcal{O}), t) + \alpha_1(\|\bar{u}\|_\infty) \\ &\quad + \alpha_2(\|\bar{v}\|_\infty) + \alpha_3(\|\bar{w}\|_\infty) + \|\bar{w}\|_\infty \\ &\leq \beta(\operatorname{dist}(x_{\mathrm{a}}(0), \mathcal{O}_{\mathrm{a}}), t) + \alpha_1(\|\bar{u}\|_\infty) \\ &\quad + \alpha_2(\|\bar{v}\|_\infty) + \alpha_3(\|\bar{w}\|_\infty) + \|\bar{w}\|_\infty \ ,\end{aligned}$$

where the second inequality follows from (d) and $\|s(t)\| \leq \|\bar{w}\|_\infty$ for all $t \geq 0$, and the last inequality follows from the first inequality of Lemma 1*(ii)*, ensuring that (c) holds. ■

Lemma 4: (b) $\Longleftrightarrow$ (e)

Proof: ($\Longrightarrow$) Assume that (b) holds. Using the first inequality of Lemma 1*(i)*, for any $k \in \mathbb{Z}_+$,

$$\begin{aligned}\|x_k - x^*\| &\leq \|x_{\mathrm{a},k} - x_{\mathrm{a}}^*\| \\ &\leq \beta(\|x_{\mathrm{a},0} - x_{\mathrm{a}}^*\|, k) + \alpha_1(\|\bar{u}\|_\infty) \\ &\quad + \alpha_2(\|\bar{v}\|_\infty) + \alpha_3(\|\bar{w}\|_\infty) \\ &\leq \beta(\|x_0 - x^*\| + \|w\|, k) + \alpha_1(\|\bar{u}\|_\infty) \\ &\quad + \alpha_2(\|\bar{v}\|_\infty) + \alpha_3(\|\bar{w}\|_\infty) \\ &\leq \beta(2\|x_0 - x^*\|, k) + \alpha_1(\|\bar{u}\|_\infty) + \alpha_2(\|\bar{v}\|_\infty) \\ &\quad + \alpha_3(\|\bar{w}\|_\infty) + \beta(2\|\bar{w}\|_\infty, 0) \ ,\end{aligned}$$

where the second inequality follows from (b), the third inequality follows from the second inequality of Lemma 1*(i)*, and the last inequality follows from [27, Lemma 14(2)] with $\epsilon = 1$. Finally, noting that $\alpha_3(\|\bar{w}\|_\infty) + \beta(2\|\bar{w}\|_\infty, 0) \in \mathcal{K}$ ensures that (e) holds.
($\Longleftarrow$) Assume that (e) holds. Using the second inequality of Lemma 1*(i)*, for any $k \in \mathbb{Z}_+$,

$$\begin{aligned}\|x_{\mathrm{a},k} - x_{\mathrm{a}}^*\| &\leq \|x_k - x^*\| + \|w\| \\ &\leq \beta(\|x_0 - x^*\|, k) + \alpha_1(\|\bar{u}\|_\infty) + \alpha_2(\|\bar{v}\|_\infty) \\ &\quad + \alpha_3(\|\bar{w}\|_\infty) + \|\bar{w}\|_\infty \\ &\leq \beta(\|x_{\mathrm{a},0} - x_{\mathrm{a}}^*\|, k) + \alpha_1(\|\bar{u}\|_\infty) + \alpha_2(\|\bar{v}\|_\infty) \\ &\quad + \alpha_3(\|\bar{w}\|_\infty) + \|\bar{w}\|_\infty \ ,\end{aligned}$$

where the second inequality follows from (e) and the last inequality follows from the first inequality of Lemma 1*(i)*, ensuring that (b) holds. ■

Lemma 5: (f) $\Longleftrightarrow$ (a)

Proof: The proof of this lemma is a direct consequence of the fact that the map P_0 in (12) and the 0-input augmented Poincaré map P_{a} in (9) are related by

$$P_{\mathrm{a}}(x_{\mathrm{a}}, 0, 0, 0) = \begin{bmatrix} P_0(x)^{\mathrm{T}} & 0^{\mathrm{T}} \end{bmatrix}^{\mathrm{T}} \ . \tag{17}$$

We only note that in proving ($\Longleftarrow$), the switching surface $\mathcal{S}_0$ corresponds to $\mathcal{S}$ evaluated at s_0 and remains constant since the lemma deals with the 0-input case. ■

Now, we are ready to present the proof of Theorem 1.

Proof: [Theorem 1] The proof of Theorem 1*(i)* $\Longleftrightarrow$ Theorem 1*(ii)* follows by using Lemmas 5, 2, and 4. The proof of Theorem 1*(i)* $\Longleftrightarrow$ Theorem 1*(iii)* follows by using Lemmas 5, 2, and 3, completing the proof of Theorem 1. ■

VI. LISS of a Bipedal Walker

In this section, we use Theorem 1 to establish LISS of limit-cycle gaits on the bipedal robot model of Fig. 2(a) that walks on uneven terrain under the influence of externally applied forces. Although in this section we work with a single limit-cycle gait, such periodic orbits can be used as *movement primitives* in a supervisory control system, the goal of which is, for example, to realize a desired motion planning objective [23] or to make the system robust against large-scale uncertainty [24]. Establishing LISS of the individual movement primitives that are made available to the supervisor is a critical component in devising provably safe switching policies that comply with the high-level objectives.

Let $q := (q_1, \cdots, q_5)$ be the configuration coordinates of the robot, labeled in Fig. 2(a), $x := (q, \dot{q}) \in \mathbb{R}^{10}$ be the state, and $u \in \mathcal{U} := \{u : \mathbb{R}_+ \to \mathbb{R}^2 \mid \|u\|_\infty < \infty,\ u \text{ is continuous}\}$ be an external force. Then, the evolution of the state during the swing phase is

$$\dot{x} = f(x) + g(x)\Gamma + g_{\mathrm{e}}(x)u \ , \tag{18}$$

where f, g, and g_{e} are the corresponding vector fields and $\Gamma \in \mathbb{R}^4$ includes the actuator inputs associated with a feedback controller; see [15, Section II.A] for exact expressions. The swing phase terminates when the swing-foot reaches the ground. We assume that the height of the ground changes changes on a step-to-step basis as shown in Fig. 2(a). Let $w \in \mathbb{R}$ represent the change in the height between consecutive steps, so that the switching surface is

$$\mathcal{S}(w) := \{(q, \dot{q}) \in \mathbb{R}^{10} \mid p_{\mathrm{E}}^{\mathrm{v}}(q) - w = 0\} \ , \tag{19}$$

where $p_{\mathrm{E}}^{\mathrm{v}}(q)$ is the height of the swing foot. Impact of the swing foot with the ground is assumed to be instantaneous and modeled as $\Delta : \mathbb{R}^{10} \times \mathbb{R}^2 \to \mathbb{R}^{10}$, which maps the states prior to impact x^- to the states post-impact x^+, under the influence of an impulsive disturbance $v \in \mathbb{R}^2$. Combining the continuous dynamics of the swing phase (18) and the discrete dynamics given by Δ, the walking cycle of the biped can be expressed as a forced SIE

$$\Sigma : \begin{cases} \dot{x} = f(x) + g(x)\Gamma + g_{\mathrm{e}}(x)u, & \text{if } x \notin \mathcal{S}(w) \\ x^+ = \Delta(x^-, v), & \text{if } x^- \in \mathcal{S}(w) \end{cases} . \tag{20}$$

The augmented SIE can be readily defined as in Section III.

An asymptotically stable periodic orbit $\mathcal{O}$ in the absence of external signals can be generated as in [15]. Then, following Section III, we obtain the discrete-time system

$$x_{k+1} = P(x_k, u_k, v_k, w_k) \ , \tag{21}$$

with a 0-input fixed point x^*, where P is the x projection of the augmented forced Poincaré map, as in (11). Then, x^* is an asymptotically stable fixed point of the map $P_0(\cdot) = P(\cdot, 0, 0, 0)$, and using Theorem 1 it follows that the 0-input fixed point x^* of (21) and the periodic orbit $\mathcal{O}$ of (20) are LISS; Figs. 2(b) and 2(c) provide a numerical verification.

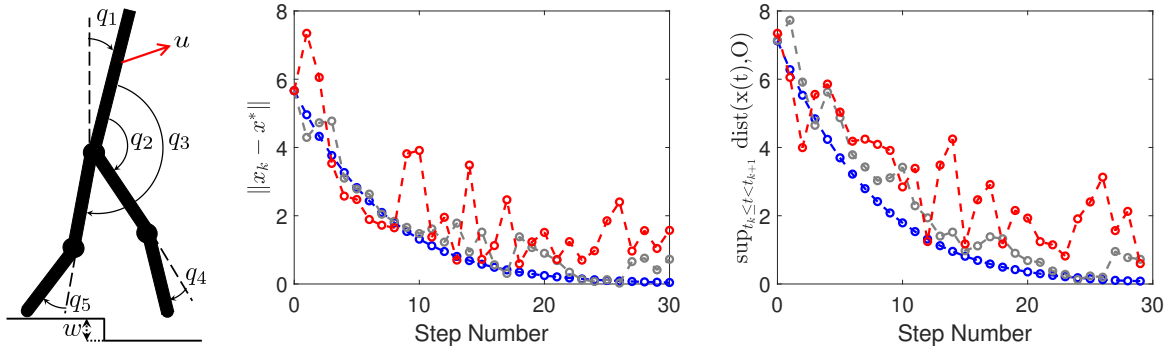

(a) (b) (c)

Fig. 2. **(a)** Robot model with a choice of generalized coordinates. **(b), (c)** Response of the biped when $u = 0$ N, $\|\bar{v}\|_\infty = 0$ N.s, $\|\bar{w}\|_\infty = 0$ cm in blue; $u = [2\sin(4t)\ 0]^{\mathrm{T}}$ N, $\|\bar{v}\|_\infty = 0.1$ N.s, $\|\bar{w}\|_\infty = 1$ cm in gray; and $u = [4\sin(4t)\ 0]^{\mathrm{T}}$ N, $\|\bar{v}\|_\infty = 0.2$ N.s, $\|\bar{w}\|_\infty = 2$ cm in red. **(a)** Evolution of $\|x_k - x^*\|$ where $\{x_k\}_{k=0}^{\infty}$ is the solution of (11) **(b)** Supremum deviation of $x(t) = \psi(t, x(0), u, \bar{v}, \bar{w})$, the solution of (20), from $\mathcal{O}$ over each step.

VII. Conclusion

In this paper, we presented a method to rigorously analyze the LISS of periodic orbits of SIEs by studying the stability properties of the fixed point of the associated Poincaré map. This greatly simplifies robustness analysis and facilitates the design of robust controllers by allowing the control designer to restrict attention to the fixed point of the discrete dynamical system given by the Poincaré map, rather than working directly with the hybrid solutions of the SIE. We studied disturbances in the continuous-time dynamics, discrete update dynamics, as well as the switching surface. The theoretical results are numerically verified in the case of an underactuated bipedal robot walking dynamically on uneven terrain under the influence of persistent external excitation.

References

[1] J. Guckenheimer and P. Holmes, *Nonlinear Oscillations, Dynamical Systems, and Bifurcations of Vector Fields*, ser. Applied Mathematical Sciences. New York: Springer-Verlag, 1996, vol. 42.

[2] W. M. Haddad, V. Chellaboina, and S. G. Nersesov, *Impulsive and hybrid dynamical systems*. Princeton, New Jersey: Princeton University Press, 2006.

[3] E. D. Sontag, "Input to state stability: Basic concepts and results," in *Nonlinear and optimal control theory*, ser. Lecture Notes in Mathematics. Springer, 2008, vol. 1932, pp. 163–220.

[4] D. Baĭnov and P. S. Simeonov, *Systems with impulse effect: stability, theory, and applications*. Chichester, U.K.: Ellis Horwood, 1989.

[5] G. Ballinger and X. Liu, "Permanence of population growth models with impulsive effects," *Mathematical and Computer Modelling*, vol. 26, no. 12, pp. 59–72, December 1997.

[6] E. R. Westervelt, J. W. Grizzle, C. Chevallereau, J. H. Choi, and B. Morris, *Feedback Control of Dynamic Bipedal Robot Locomotion*. Boca Raton, FL: CRC Press, 2007.

[7] R. D. Gregg and M. W. Spong, "Reduction-based control of three-dimensional bipedal walking robots," *Int. J. of Robotics Research*, vol. 29, no. 6, p. 680702, 2009.

[8] L. B. Freidovich, U. Mettin, A. S. Shiriaev, and M. W. Spong, "A passive 2-DOF walker: Hunting for gaits using virtual holonomic constraints," *IEEE Tr. on Robotics*, vol. 25, no. 5, pp. 1202–1208, 2009.

[9] S. Kolathaya and A. D. Ames, "Parameter to state stability of Control Lyapunov Functions for hybrid system models of robots," *Nonlinear Analysis: Hybrid Systems*, vol. 25, pp. 174–191, 2017.

[10] Q. Nguyen and K. Sreenath, "Optimal robust control for bipedal robots through control lyapunov function based quadratic programs," in *Proc. of Robotics: Science and Systems*, 2015.

[11] K. A. Hamed and R. D. Gregg, "Decentralized event-based controllers for robust stabilization of hybrid periodic orbits: Application to underactuated 3d bipedal walking," *IEEE Tr. on Automatic Control*, 2018.

[12] C. O. Saglam and K. Byl, "Robust policies via meshing for metastable rough terrain walking," in *Proc. of Robotics: Science and Systems*, 2014.

[13] B. Griffin and J. Grizzle, "Walking gait optimization for accommodation of unknown terrain height variations," in *Proc. of American Control Conf.*, 2015, pp. 4810–4817.

[14] K. A. Hamed, B. G. Buss, and J. W. Grizzle, "Exponentially stabilizing continuous-time controllers for periodic orbits of hybrid systems: Application to bipedal locomotion with ground height variations," *Int. J. of Robotics Research*, vol. 35, no. 8, pp. 977–999, 2016.

[15] S. Veer, M. S. Motahar, and I. Poulakakis, "On the adaptation of dynamic walking to persistent external forcing using hybrid zero dynamics control," in *Proc. of IEEE/RSJ Int. Conf. on Intelligent Robots and Systems*, 2015, pp. 997–1003.

[16] M. S. Motahar, S. Veer, J. Huang, and I. Poulakakis, "Integrating dynamic walking and arm impedance control for cooperative transportation," in *Proc. of IEEE/RSJ Int. Conf. on Intelligent Robots and Systems*, 2015, pp. 1004–1010.

[17] S. Veer, M. S. Motahar, and I. Poulakakis, "Local input-to-state stability of dynamic walking under persistent external excitation using hybrid zero dynamics," in *Proc. of American Control Conference*, 2016, pp. 4801–4806.

[18] M. S. Motahar, S. Veer, and I. Poulakakis, "Steering a 3d limit-cycle walker for collaboration with a leader," in *Proc. of IEEE/RSJ Int. Conf. on Intelligent Robots and Systems*, 2017, pp. 5251–5256.

[19] E. D. Sontag and Y. Wang, "New characterizations of input-to-state stability," *IEEE Tr. on Automatic Control*, vol. 41, no. 9, pp. 1283–1294, 1996.

[20] C. Cai and A. R. Teel, "Characterizations of input-to-state stability for hybrid systems," *Systems & Control Letters*, vol. 58, no. 1, pp. 47–53, January 2009.

[21] S. Veer, Rakesh, and I. Poulakakis, "Input-to-state stability of periodic orbits of systems with impulse effects via Poincaré analysis," *IEEE Tr. on Automatic Control*, 2019, to appear. Available through arXiv preprint, arXiv:1712.03291.

[22] R. R. Burridge, A. A. Rizzi, and D. E. Koditschek, "Sequential composition of dynamically dexterous robot behaviors," *Int. J. of Robotics Research*, vol. 18, no. 6, pp. 534–555, 1999.

[23] M. S. Motahar, S. Veer, and I. Poulakakis, "Composing limit cycles for motion planning of 3D bipedal walkers," in *Proc. of IEEE Conf. on Decision and Control*, 2016, pp. 6368–6374.

[24] S. Veer, M. S. Motahar, and I. Poulakakis, "Adaptation of limit-cycle walkers for collaborative tasks: A supervisory switching control approach," in *Proc. of IEEE/RSJ Int. Conf. on Intelligent Robots and Systems*, 2017, pp. 5840–5845.

[25] S. Veer and I. Poulakakis, "Safe adaptive switching among dynamical movement primitives: Application to 3D limit-cycle walkers," in *Proc. of IEEE Int. Conf. on Robotics and Automation*, 2019.

[26] H. K. Khalil, *Nonlinear Systems*, 3rd ed. Upper Saddle River, New Jersey: Prentice hall, 2002.

[27] E. Sarkans and H. Logemann, "Input-to-state stability of discrete-time Lur'e systems," *SIAM Journal on Control and Optimization*, vol. 54, no. 3, pp. 1739–1768, 2016.